Title

Head Movements Control the Activity of Primary Visual Cortex in a Luminance-Dependent Manner

Journal

Neuron, 108(3)

ISSN

0896-6273

Authors

Bouvier, Guy
Senzai, Yuta
Scanziani, Massimo

Publication Date

2020-11-01

DOI

10.1016/j.neuron.2020.07.004

Peer reviewed

HHS Public Access

Author manuscript

Neuron. Author manuscript; available in PMC 2021 November 11.

Published in final edited form as:

Neuron. 2020 November 11; 108(3): 500–511.e5. doi:10.1016/j.neuron.2020.07.004.

Head movements Control the Activity of Primary Visual Cortex in a Luminance Dependent Manner

Guy Bouvier[1,2,*], **Yuta Senzai**[1,2], **Massimo Scanziani**[1,2,3,*]

[1]Department of Physiology, University of California San Francisco, San Francisco, CA, USA.

[2]Howard Hughes Medical Institute, University of California San Francisco, San Francisco, CA, USA

[3]Lead Contact

Summary

The vestibular system broadcasts head-movement related signals to sensory areas throughout the brain, including visual cortex. These signals are crucial for the brain's ability to assess whether motion of the visual scene results from the animal's head-movements. How head-movements impact visual cortical circuits remains, however, poorly understood. Here, we discover that ambient luminance profoundly transforms how mouse primary visual cortex (V1) processes head-movements. While in darkness, head movements result in an overall suppression of neuronal activity, in ambient light the same head movements trigger excitation across all cortical layers. This light-dependent switch in how V1 processes head-movements is controlled by somatostatin-expressing (SOM) inhibitory neurons, which are excited by head movements in dark but not in light. This study thus reveals a light-dependent switch in the response of V1 to head-movements and identifies a circuit in which SOM cells are key integrators of vestibular and luminance signals.

In Brief

The vestibular system broadcasts head-movement related signals throughout the brain. Bouvier et al. show that ambient light impacts how primary visual cortex (V1) responds to head-movements. V1 is suppressed by head movements in darkness and excited by head-movements in light through the differential recruitment of somatostatin-expressing inhibitory neurons.

Keywords

visual cortex; vestibular system; somatostatin interneurons; luminance; head movements

[*]Correspondence: bouvier.ga@gmail.com & massimo@ucsf.edu.

Author Contributions

G.B. and M.S. designed experiments and wrote the manuscript. G.B. performed all the experiments, except Y.S. implanted the chronic electrodes. G.B. analyzed the data.

Competing interests

The authors declare no competing interests.

Introduction

Primary sensory areas of the mammalian cortex are each dedicated to one sensory modality defined by the sensory organs they receive input from. The vestibular organs detect angular rotation and linear acceleration of the head, and transmit these signals to the brain (Angelaki, 2004; Angelaki and Cullen, 2008). However, unlike most other senses, no primary cortical area is dedicated to the processing of vestibular signals. Instead, head-movement related signals are broadcast across cortical areas dedicated to distinct sensory modalities (Duffy, 1998; Vanni-Mercier and Magnin, 1982; Rancz et al., 2015; Vélez-Fort et al., 2018). The integration of vestibular signals with other sensory modalities likely allows the brain to assess whether a given sensory stimulus results from the animal's head movement in the environment rather than from a change in the sensory environment itself. Primary visual cortex (V1) of the mouse is one of those sensory areas which, in addition to receiving input from their main sensory organ, the retina, also receives head-movement related signals from vestibular organs (Vélez-Fort et al., 2018). While we have extensive knowledge of how cortical circuits in V1 process visual stimuli, we still have only a rudimentary understanding of how those same visual circuits process vestibular signals.

Prior work on the impact of vestibular stimuli on activity in visual cortex has led to different observations. Studies in humans indicate that vestibular stimulation reduces basal activity in visual cortex, implying an overall suppressive effect of the vestibular system on this structure (Bense et al., 2001; Wenzel et al., 1996). However, more recent work in mice V1 has shown that head movements increase activity in layer 6 pyramidal neurons, instead implying an excitatory effect, at least in this layer (Vélez-Fort et al., 2018). Other studies in primates and carnivores have shown more heterogeneous and complex effects of vestibular stimulation on visual cortex activity, depending on the type of vestibular stimuli and the properties of the visual stimuli presented concomitantly to the vestibular stimulus (Duffy, 1998; Gu et al., 2006; Vanni-Mercier and Magnin, 1982; Ohshiro et al., 2017). The impact of vestibular stimuli on V1 may also depend on ambient luminance. In fact, V1 has been shown to adapt to changes in luminance through sustained changes in its basal activity (Kayama et al., 1979; Kinoshita and Komatsu, 2001; Tucker and Fitzpatrick, 2006; Xing et al., 2014). Thus, depending on ambient luminance V1 may differentially process incoming vestibular information.

Here, using extracellular recordings in head-fixed and freely moving mice, we show that head movements control V1 activity in a luminance-dependent manner. In the dark, head movements exert an overall suppressive action on neuronal activity in V1 while in light, the same head movements robustly shift cortical activity toward excitation. This light-mediated shift in vestibular responses impacts both pyramidal cells and parvalbumin-expressing (PV) inhibitory cells in a similar manner, while exerting an opposite effect on somatostatin expressing (SOM) inhibitory cells. Finally, we show that ablation of SOM cells strongly reduces both the suppression of V1 in response to head movements in the dark and the shift toward excitation in light. This study reveals a light-dependent vestibular impact on V1 and identifies a circuit in which SOM cells are key integrators of vestibular and luminance signals.

Results

Suppression of V1 by head movements in the dark

How does V1 respond to head movements? To control the velocity and amplitude of head movements, we fixed the head of awake mice in the center of a servo-controlled table enabling the rotation of the animal along the horizontal plane (50° rotation; 80°/s peak velocity; unless stated otherwise Figure 1A). Using extracellular linear probes, we recorded from neurons in the left V1 across all cortical layers in complete darkness (see STAR Methods).

The firing rate of most V1 neurons (62%; 928 out of 1502 cells; n = 30 mice) was modulated by either clockwise (CW; contraversive) or counterclockwise (CCW; ipsiversive) rotations of the table (Figure 1B, Figure S1A-C). The time-course of this modulation approximated the velocity profile of the rotating table (Figure 1C and S1G) and 40% of the modulated neurons showed a significant difference in the response to CW or CCW rotations (Figure S1A-E). We quantified the response of V1 neurons by computing the vestibular modulation index (vMI, Figure 1D, top panel). Positive or negative vMIs indicate, respectively, an increase (excitation) or decrease (suppression) in activity relative to baseline (Figure S1F). Strikingly, both CW and CCW rotations led to a strong overall suppression of neuronal activity, particularly in the superficial layers (layer 2/3 and layer 4; Figure 1C,D and S1B,C). In contrast, neurons in deep layers (layer 5 and layer 6) were approximately equally distributed between those that were suppressed and those that were excited (Figure 1C,D and S1B,C). This was the case for both regular-spiking (RS; putative excitatory cells, Figure 1) and fast-spiking cells (FS; putative PV cells, Figure S2A-D). Furthermore, the overall suppressive impact of head movements on V1 activity was observed independently of the specific velocity profile or peak velocity used to rotate the table (Figure S1H). Because both the fraction of modulated cells (Figure S1B,C) and the vMIs were similar for CW and CCW rotations (CW vs. CCW vMI, Superficial layers vMI: −0.44±0.02 vs - 0.48±0.02, n = 404 cells; Deep layers vMI: −0.12±0.01 vs −0.15±0.01, n = 1098 cells; 30 mice), we focused on CW rotations exclusively.

The response of V1 neurons to table rotations depended on the vestibular organ because bilateral vestibular lesions abolished the response (Figure 1E). Moreover, even though V1 can respond to sound (Iurilli et al., 2012; Deneux et al., 2019), the response to table rotations was not due to the sound of the servo motor because detaching the table from the motor, hence preserving the sound without triggering rotation, did not elicit any response (3.8%, 13/341 cells, n = 3 mice, data not shown).

Taken together, these data show that head movements control the activity of large fractions of V1 neurons across all layers and exert an overall suppressive impact, especially in superficial layers.

Excitation of V1 by head movements in light

Because V1 basal activity is regulated by ambient luminance (Kayama et al., 1979; Kinoshita and Komatsu, 2001; Tucker and Fitzpatrick, 2006; Xing et al., 2014), we compared the response of V1 to head movements in dark and light conditions. To avoid

contaminating V1 responses to head movements in light with responses to the visual environment, we stitched both eyelids and placed a light diffuser between the light source and the animal's right eye (contralateral to the recorded V1) to achieve a homogeneous illumination of the eye (Figure 2A, see STAR Methods). We alternated rotations in light and dark conditions.

Light itself, i.e. prior to table rotation, had a suppressive impact on the basal activity of V1 neurons in superficial layers, consistent with previous reports (Tucker and Fitzpatrick, 2006; Xing et al., 2014; Figure 2B,C for RS cells and S2E-G for FS cells) and a facilitating impact on the basal activity of neurons in deep layers. We quantified the impact of light on basal activity using the luminance modulation index (lumMI; positive or negative lumMIs indicate a light mediated increase or a decrease in basal activity relative to dark, respectively).

In striking contrast to the suppressive impact of head movements in the dark, head movements in the light resulted in an overall excitation of V1 cells (Figure 2D,E and S2H,I). Not only did light increase the average vMI across all layers, but cells in superficial layers shifted from a net average suppression in the dark to a net average excitation by head movements in light (Figure 2D-F, S2H-J and S3A-D). Despite this strong shift towards excitation, the preference of individual neurons for CW or CCW rotations remained essentially unaltered (Figure S3E). Consistent with the population average data, the response to head movements of most individual cells shifted towards positive vMIs in light as compared to dark (Figure S3A-D). Interestingly, this shift towards positive vMI depended on the impact of light on the cell's basal activity: the larger the light mediated suppression of basal activity, the larger the positive shift of the vMI. This was the case for both RS and FS cells (Figure 2G and S2K). However, the overall increase in vMI did not simply result from a flooring effect due to the reduction in basal activity by light. This is exemplified by the large fraction of neurons whose head-movement mediated suppression in the dark switched to net excitation in light, rather than just to a reduction in suppression (Figure S3A; cells in the upper left quadrant). Hereinafter, we refer to the positive shift of vMI from dark to light as facilitation.

The impact of light on basal activity and on the vMI persisted for as long as illumination continued. Even in light-adapted mice (see STAR Methods) vMI remained positively shifted relative to the vMI measured in the same dark-adapted mice (Figure S4A-E). The same was true also for the light-induced change in basal activity (Figure S4F). That is, basal activity remained lower in superficial layer and higher in deep layers as compared to dark-adapted conditions for as long as the light was on (up to 25 min).

It is conceivable that reflexive eye movements induced by the rotation of the table, by changing some residual luminance pattern on the retina, may trigger a visual response in V1 (Akerman et al., 2002; Krug et al., 2001). To control for this possibility, we blocked eye movements (Figure S4G; see STAR Methods) and compared V1 activity in response to head movements in dark and light (Figure S4H,I). Even after abolishing eye movements, the response in V1 to head movements shifted from overall suppression to overall excitation (Figure S4H,I). This indicates that putative, eye movement-induced local changes in luminance on the retina do not substantially contribute to the facilitation of the V1 response.

These data thus show that head movements control the activity of V1 neurons in a luminance-dependent manner. While head movements mainly suppress V1 neurons in the dark, the same head movements in light excite V1 neurons.

Excitation of layer 5 SOM cells by head movements in dark but not in light.

What is the source of V1 suppression in response to head movements in the dark and how is this suppression reduced in light? An inhibitory neuron who is excited by head movements in the dark, thereby suppressing its targets, but is no longer excited by the same head movements in light, could account for the observed phenomena. The two main classes of inhibitory neurons targeting RS cells in V1 are PV and SOM expressing cells (Pfeffer et al., 2013).

As described above (Figure S2) a fraction of FS cells (putative PV expressing cells), mainly those located in deep layers, were excited by head movements in the dark, potentially accounting for the suppression of V1 neurons across cortical layers (Bortone et al., 2014). However, those same FS cells were equally excited by head movements in light (Dark vs Light: vMI: 0.31±0.03 vs 0.25±0.04, n = 55 cells, P = 0.1, Figure S2I). Thus, PV cells are unlikely to mediate that component of V1 suppression to head movements that is relieved by light. We thus turned to SOM cells.

To isolate the response of V1 SOM cells to head movements, we opto-tagged these neurons via the conditional expression of Channelrhodopsin 2 in SOM-Cre mice (Lima et al., 2009). Like RS and FS cells, SOM cells in the superficial layers were on average suppressed by head movements in the dark, and excited by head movements in light (Figure 3A-C). Therefore, like FS cells, superficial SOM cells are unlikely candidates for the head-movement mediated suppression of V1 neurons in the dark and their facilitation by light. In contrast, however, SOM cells in deep layers were excited by head movements in dark and suppressed by the same head movements in light (Figure 3B,C). Thus, unlike RS and FS cells, light decreased their vMI. Furthermore, in response to light, i.e. prior to table rotations, the basal activity of these deep-SOM cells increased (Figure 3D,E), again unlike RS and FS cells. In fact, the larger the increase in their basal activity by light, the larger their decrease in vMI (Figure 3F). These results show that SOM cells in deep layers are excited by light as well as by head movements in the dark, and that light occludes their excitation to head movements.

This observation makes SOM cells in deep layers potential candidates for the suppression of V1 neurons by head movement in dark and the facilitation by head movement in light. This result also makes deep-layer SOM cells potential candidates for the suppression of the basal activity of V1 neurons by light.

SOM cells suppress V1 neurons in response to head movements in dark but not in light

To directly test the involvement of SOM cells in the head-movement mediated suppression of V1 neurons, we specifically ablated these cells in V1 through the conditional expression of Caspase-3 in SOM-Cre x Ai14 mice. This resulted in a 86.5±0.02% reduction of SOM cells compared to the contralateral non-injected hemisphere (Figure 4B, see STAR Methods)

and in a slight increase in basal activity of RS cells (control average FR = 2.87±0.16Hz, SOM ablation FR = 3.30±0.17Hz, P = 0.0004).

Ablation of SOM cells significantly reduced the head-movement mediated suppression of V1 neurons in the dark, reversed the suppressive impact of light on basal activity, and reduced the facilitation of the V1 response to head movements in light (Figure 4, 5, and S5). The reduction of head-movement mediated suppression in dark was particularly prominent for RS and FS cells in superficial layers (Figure 4 and S5A-D, respectively). SOM cell ablation also profoundly impacted the light-mediated suppression of V1 basal activity (Figure 5A-D for RS cells and S5E-H for FS cells). In Caspase-3 injected mice, light increased instead of suppressing basal activity (Figure 5A-D and S5E-H for FS cells). If the relationship between the light-mediated suppression of basal activity and the facilitation of the response to head movements is causal, reducing the impact of light on basal firing rate should decrease the facilitation of the response to head movements by light. Indeed, facilitation of responses to head movements in light was strongly reduced in SOM cell ablated mice, as compared to their control littermates (Figure 5E-H).

Taken together, these data show that the suppression of V1 neurons by head movements in dark and the dependence of this suppression on ambient luminance relies in large part on SOM cells: SOM cells suppress V1 neurons in response to head movements in dark and, by releasing their suppression in light, enable facilitation of the response. Thus, while V1 still strongly responds to head movements following SOM cell ablation, this response is much less dependent on luminance (Figure 5H). Furthermore, these data show that SOM cells also suppress V1 basal activity in response to light, thus explaining the observed relationship between the magnitude of suppression of basal activity by light and the degree of facilitation of the response to head movements (Figure 2G for RS cells and S2K for FS cells).

PV and 5HT3aR cells do not contribute to the suppression of V1 by head movements

We verified that the impact of SOM cell ablation on head movement and light responses in V1 was not due to a nonspecific decrease in inhibition, by selectively ablating PV cells and 5-Hydroxytryptamine3a receptor (5HT3aR) expressing inhibitory cells which, together with SOM cells, account for nearly 100% of inhibitory neurons in cortex (Lee et al., 2010). We confirmed the ablation of PV cells both histologically (92±0.04% ablated PV cells) and by the reduction of recorded FS cells (11±2.2% vs 2.9±1.2%, P = 0.03; n = 5 mice for both). Ablation of PV cells led to a small increase in basal activity as compared to non-injected areas in V1 (2.46±0.29 Hz vs 2.91±0.14 Hz, P = 0.003). Ablation of 5HT3aR cells reduced this neuronal population by 86.2±0.008% without any significant impact on basal activity of RS cells (2.80±0.16Hz vs 2.69±0.14Hz, control: n = 8 mice; 5HT3aR cell ablation: n = 11 mice).

Neither PV nor 5HT3aR cell ablation significantly affected the response of RS cells to head movements (Figure S6A-D and S6E-H, respectively). Moreover, neither PV nor 5HT3aR cell ablation impacted the suppression of basal activity by light (PV control: lumMI = −0.21±0.03; n = 272 cells; 5 mice; PV ablation: lumMI = −0.16±0.03; n = 253 cells; 4 mice; p = 0.17; 5HT3aR control: lumMI = −0.22±0.02; n = 631 cells; 10 mice; 5HT3aR ablation: lumMI = −0.18±0.02; n = 583 cells; 10 mice; p = 0.22). Therefore, PV and 5HT3aR cells do

not significantly contribute to either the head-movements mediated suppression of RS cells or to the light-mediated suppression of their basal activity. These results highlight the unique role of SOM cells in the suppression of V1 by head movements in dark, the relief of suppression to head movements in light, and the suppression of V1 basal activity by light.

Light-mediated facilitation of V1 activity to head movements in freely moving mice

Although head-fixed mice on a rotating table allow us to stimulate the vestibular organs through controlled head movements, in freely moving mice the vestibular signal arise from head movements initiated by the animal. To determine whether these active head movements impact V1 activity in a similar manner as observed in response to passive head movements, we performed electrophysiological recordings from V1 in freely moving mice. We recorded the angular velocity of head movements using an inertial measurement unit (IMU) attached to the head of the mouse (Figure 6A, see STAR Methods). As above, the eyelids were sutured to prevent patterned visual stimulation, and dark/light conditions were alternated every two minutes. Spontaneous exploratory behavior was accompanied by a wide range of head angular velocities along the three orthogonal planes captured by the IMU, with higher velocities for the horizontal component of the head movements (yaw) (Figure 6B). The distribution of angular velocities was similar in dark and light conditions (yaw average head angular velocity in dark vs. light: 46.7±4.0 °/s vs 46.8±5.5 °/s, P = 1, n = 4 mice). To characterize the relationship of firing rate to angular velocity, we calculated the head rotation modulation index (hrMI) for yaw rotations (see STAR Methods). A large fraction of V1 cells (53%) was significantly modulated by angular velocity in the dark, around any plane and direction and 49% of cells specifically by head motions with a yaw component (CW and CCW). Consistent with head fixed conditions, average V1 activity was suppressed by active head movements in the dark, with a more robust suppression of cells in superficial layers (Figure 6C,D). Furthermore, head movements in light resulted in an overall shift towards facilitatory responses leading to and a 25±8% decrease in suppressed cells and a 33.3±11.8% increase in facilitated cells (Figure 6E).

These results show that active head movements control the activity of large fractions of V1 neurons in a luminance-dependent manner. On one hand, active head movements in the dark suppress, on average, V1 neurons, similar to passive head movements triggered by table rotations. Active head movements in light, on the other hand, excite, on average, V1 neurons, again similar to passive head movements.

Discussion

Movements of an animal through its environment continuously activate the animal’s vestibular system whose signals are broadcast throughout the brain, including visual cortex. These signals are believed to contribute to the organism’s ability to distinguish between sensory stimuli resulting from the animal’s movements from those resulting from an actual change in the environment. This study reveals a light-dependent switch in the response of V1 to head movements and identifies a circuit in which SOM cells are key integrators of vestibular and luminance signals.

The strong suppression of V1 by head movements in darkness may act as a veto in the processing of visual stimuli, for example the shift of the visual scene as the animal moves its head, that are unreliable due to dim ambient luminance conditions. In contrast, excitation of V1 by head movement in light may contribute to the combination of visual and vestibular signals as the animal navigates through its environment in bright conditions, possibly enabling visual cortex to attribute shifts in the visual scene to head movements of the animal.

To understand how and whether the responses of V1 to head movements contribute to the ability of V1 to discriminate between visual flow resulting from the animal's movements from movements occurring in the environment, future work will need to correlate the response properties of individual neurons to head movements with those of the same neurons to visual flow. One can imagine a scenario in which the vestibular stimulus produced by a head movement, say in the CW direction (hence resulting in a CCW visual flow), activates neurons with a preference for CW visual flow. As a consequence, CW head movements in the presence of patterned vision would activate neuronal populations tuned to the two opposite directions of visual flow, one responding to the actual CCW visual flow, the other to the vestibular stimulus. This would lead to a net cancellation of the population response to a specific direction of visual flow. Consistent with this hypothesis, in the dorsal medial superior temporal cortex as well as in the ventral parietal cortex, most of the cells have the same preferred direction to head rotation in the dark and for visual flow (Bremmer et al., 2002; Takahashi et al., 2007). Alternatively, head movements in a given direction may trigger responses that are uncorrelated with the response of the neurons to the direction of visual flow. In this case, the nature of the stimulus (whether generated by head motion or movements in the environment) may be sorted out by downstream areas targeted by these neurons.

Elegant work in the mouse V1 first demonstrated the excitatory impact of head movements, especially in neurons located in deep layers (Velez-Fort et al., 2018), a finding reproduced in the present study. The same study, however, did not report the suppression in superficial layers. Given the low basal firing rates of neurons in superficial layers, and hence the large number of repetitions necessary to observe a suppressive effect, it is possible that the suppression remained undetected. Recent work focusing on layer 2/3 neurons in freely moving rats, shows the suppression of neurons by head movements in the dark, and a shift towards excitation in light, thus consistent with the present work (Guitchounts et al., 2020).

What is the mechanism of suppression of V1 neurons by head movements? Work from our lab demonstrated the presence of translaminar FS cells (putative PV cells) whose somata and dendrites are located in deep layers and whose axons arborize in superficial layers (Bortone et al. 2014), and thus represented a candidate inhibitory neuron to suppress cells in superficial layers. Two lines of evidence argue against this possibility: First, deep layer FS cells were equally excited by head movements in dark and light while the candidate inhibitory neurons response to head movements in light should be reduced. Second, ablation of PV cells did not affect head-movement mediated suppression of neurons in the dark. Thus, FS cells in general, and translaminar FS cells in particular, do not contribute to the suppression of V1 by head movements in darkness.

Because head movements and light similarly impacted RS and FS cells, and both RS and FS cells are targeted by SOM cells (Pfeffer et al., 2013), we reasoned that the SOM cells may be a potential candidate for both the head-movements and the light mediated suppression of V1 activity. Indeed, deep-layer SOM cells increased their firing rate in response to head movements in dark and in response to light onset, as would be expected for neurons suppressing their targets in response to these two distinct stimuli. Further supporting this possibility, SOM cell ablation reduced both the head-movement and the light mediated suppression of basal activity in RS and FS cells. Thus, our data show that SOM cells contribute to the head-movement mediated suppression of V1 neurons in the dark. Importantly, our data also demonstrate that SOM cells represent the basis for the light mediated suppression of basal activity in V1 (Tucker and Fitzpatrick, 2006; Xing et al., 2014).

Upon ablating SOM cells, we not only removed the light-mediated suppression of RS and FS basal firing rate, but also reduced the facilitation of their response to head movements by light. Thus, SOM cells represent the causal link between the light-mediated decrease in basal firing rate and the correlated facilitation of responses to head movements observed in V1 neurons. By comparing the activity of SOM cells across layers, only SOM cells in deep layers were excited in response to head movements in the dark, no longer so in light, and increased their basal activity in light. These SOM cells are likely deep layer Martinotti cells, because of their location and spike shape (Ma et al., 2006; Naka et al., 2019; Nigro et al., 2018, see STAR Methods). Therefore, we propose that deep layer Martinotti cells integrate vestibular and luminance signals in V1.

Clearly, SOM cells contribute to only part of the vestibular modulation of V1 neuron activity. SOM cells do not contribute to the direct excitation of V1 neurons in response to head movements and their ablation does not eliminate all head-motion mediated suppression. Future work will determine the source of vestibular input onto V1 in general and onto SOM cells specifically. It has been suggested that retrosplenial cortex is a source of vestibular input to V1 (Vélez-Fort et al., 2018), but several other areas responding to vestibular stimulation and projecting to V1 may also contribute (Leinweber et al., 2017; Rancz et al., 2015; Wang and Burkhalter, 2007). Also, the nature of the luminance input onto SOM cells remains to be established. While a large fraction of neurons in the dorsolateral geniculate nucleus of the thalamus (dLGN), the primary visual input to V1, increases firing in response to increases in luminance (Storchi et al., 2017; Tucker and Fitzpatrick, 2006), SOM cells are not a major target for dLGN afferents (Ji et al., 2016).

Irrespective of the exact origin of the inputs, our data indicate that SOM cells are integrators of head movements and luminance. Interestingly, other non-visual modulations of V1 activity have been shown to be affected by light, like the response of V1 to auditory stimuli (Deneux et al., 2019). Future work will determine whether SOM cells represent a general mechanism for the luminance dependence of non-visual responses in V1.

Despite the overall suppression of V1 in response to head movements in the dark and the overall excitation in light, the magnitude of suppression or excitation varied across individual neurons, (Figure S3A). This variability may reflect the different tuning properties

of individual cells for different axes of head motion, a possibility that will be tested by moving the animal along different planes. This variability may also correlate with the tuning properties of individual neurons to visual stimuli, a possibility that can be determined by comparing the response of individual neurons to head movements with their visual tuning properties.

Head movements in freely moving mice triggered responses in V1 that were similar to those triggered by passive head movements in head-fixed mice, and these responses were also modulated by light, consistent with recent work (Guitchounts et al., 2020). The magnitude of the modulation and of the shift were, however, less pronounced in freely moving mice. This may be because V1 responds differently to passive as compared to self-initiated head movements. This may also be because head movements in head free mice did not occur along the horizontal plane exclusively, like in head fixed conditions, and we do not know how the representations along various dimensions interact in V1. Furthermore, we also do not know whether V1 response to head movements in head-free conditions exclusively represented a vestibular input or also a motor efference copy or proprio-receptive signal.

In conclusion, our work reveals that head motion exerts a strong control on the activity of V1 neurons in a layer and cell-type specific manner, and that ambient luminance controls the sign and magnitude of this impact through SOM cells. The impact of the vestibular system on V1 and its luminance dependence suggest that the landscape of activity in V1 changes continuously with the temporal dynamics of the animal's motion through its environment. An ethological understanding of how V1 processes visual information will, thus, necessitate a thorough elucidation of how these head movement generated moment-to-moment fluctuations in V1 activity are integrated with the ongoing flow of visual signals.

STAR Methods

RESOURCE AVAILABILITY

Lead contact—Further information and requests for resources and reagents should be directed to and will be fulfilled by the Lead Contacts, Massimo Scanziani (massimo@ucsf.edu).

Materials Availability—This study did not generate new unique reagents or mouse lines.

Data and Code Availability—The datasets/code generated in the current study have not been uploaded to a public repository because of large file size, but are available upon reasonable request.

EXPERIMENTAL MODEL AND SUBJECT DETAILS

Mice—All experimental procedures were conducted in accordance with the regulations of the Institutional Animal Care and Use Committee (IACUC, AN179056) of the University of California, San Francisco. All mice were housed on a reversed cycle (light/dark cycle 12/12 h) with free access to food. Data were collected from male or female C57BL/6J mice or from heterozygous mice kept on a C57BL/6J background with the following genotype:

SOM-Cre (JAX:028864) and SOM-Cre x Ai32 (JAX:024109) for photo-tagging experiments (Figure 3); SOM-Cre x Ai14 (JAX:007914) for SOM cells ablation experiments (Figure 4, 5, and S5); PV-Cre (JAX:017320) x Ai14 for PV cells ablation experiments (Figure S6), 5HT3a-Cre (MMRRC:036680-UCD) x Ai14 for 5HT3a cells ablation experiments (Figure S6). At the start of the experiments, all mice were between 2 and 7 months old.

METHOD DETAILS

Viruses—The following adeno-associated viruses (AAV) were used: AAV1-EF1a-flex-taCasp3-TEVp (final titer: $2.1.10^{12}$ genome copies/ml, Univ. of North Carolina Viral Vector Core) and AAV1-EF1a-DIO-hChR2(H134R)-EYFP (final titer: 4.10^{12} genome copies/ml, Univ. of Pennsylvania Viral Vector Core).

Surgical procedures

Viral Injections: Mice were anesthetized with 2% isoflurane and placed in a stereotactic apparatus (Kopf). Core body temperature was monitored with a rectal probe and maintained constant at 37°C with a heating pad (FHC). A thin layer of lubricant ointment (Rugby Laboratories) was applied to the eye, the head was shaved and disinfected with povidone iodine, and 2% lidocaine solution was administered subcutaneously at the incision site. A craniotomy (approx. 300 μm in diameter) was performed with a micro-burr (Gesswein) mounted on a dental drill (Foredom). Viral suspensions were loaded in beveled glass capillaries (tip diameter: 15-30 μm) and injected with a micropump (UMP-3, WPI) at a rate of 20-30 nl/minute into the parenchyma. The coordinates of the injection sites and the volumes of the injected viral suspension are detailed below. The pipette was removed from the brain 10 minutes after the completion of the injection, the head plate was attached just after the virus injection, and 0.1 mg/kg buprenorphine was administered subcutaneously as a postoperative analgesic.

This virus was injected in the left V1 at 3 sites forming a triangle (coordinates relative to the sagittal and lambdoid suture, respectively: 2300 μm lateral and 450 μm anterior; 2800 μm lateral and 450 μm anterior; 2550 μm lateral and 800 μm anterior) at 2 depths for every injection site (250 and 500 μm). Experiments were performed at least 3 weeks after the virus injection. For PV cell ablations (AAV1-EF1a-flex-taCasp3-TEVp injection in PV-Cre x Ai14 mice), we injected only one site and two depth (250 and 500 μm) to reduce the extent of PV cells ablation, and hence minimize the risk of epileptiform activity in V1.

Eyelid Suturing: Mice were anesthetized with 2% isoflurane. The eye was flushed, and eyelids swabbed with diluted betadine ophthalmic solution. Proparacaine ophthalmic solution was applied to numb the eye. The eyelid margins were sutured closed with 1 mattress suture using either polypropylene or vicryl suture.

Eye muscles resection: Mice were anesthetized with 2% isoflurane and placed on a heating pad. The eye was flushed, and eyelids swabbed with diluted betadine ophthalmic solution. Proparacaine ophthalmic solution was applied to numb the eye. Approximately 10 μl of 0.5% Lidocaine solution was injected into the conjunctiva over both medial and lateral rectus muscles. The eye was slightly displaced from the orbit using a micro-spatula, and the

lateral and then medial rectus muscles resected using micro-scissors. A 30-gauge syringe was positioned inside the eye socket under the eyeball to deposit a drop (10 μl of tissue adhesive (Vetbond, veterinary grade, 3M; Mace et al., 2018). Eye gel was applied to prevent corneal dehydration. The blockade of eye movements was verified and confirmed in a subset of mice after 1-2 hours of recovery in their home cage (Figure S4G). In mice used for electrophysiological recordings, the eye lids were sutured after the rectus muscles resection, eye movements were not monitored, and recordings were performed after 1 to 2 days of recovery in their home cage (Figure S4H,I).

Head Plate Implantation for Head-fixed Recordings: Mice were implanted with a T-shaped head-bar at least 2.5 weeks before the day of the recording. Mice were anesthetized with 2% isoflurane, the scalp was removed, the skull was disinfected with alcohol and povidone iodine, and scored with bone scraper. The edge of the skin was glued to the skull and the metal head-bar was sterilized and mounted using dental cement (Ortho-Jet powder; Lang Dental) mixed with black paint (iron oxide), or Relyx Unicem2 automix (3M ESPE). The head-bar was stereotactically mounted with the help of an inclinometer (Digi-Key electronics 551-1002-1-ND). The inclinometer allowed us to adjust the angle of the head bar in relation to the sagittal and medio-lateral axes of the head. Following the bar implantation, black dental cement was used to build a recording well surrounding the recording site. The surface of the skull above the left visual cortex was not covered with dental cement but was coated with a thin layer of transparent cyanoacrylate glue. Mice were injected subcutaneously with 0.1 mg/kg buprenorphine and checked daily after the head-bar surgery. For at least 4 days before recording, mice were habituated to head fixation within the recording setup.

Craniotomy for Electrophysiological Recordings: On the day before recording, mice were anesthetized with 2% isoflurane and the skull above the recording sites was drilled off. The dura was not removed, and the exposed brain was kept moist with artificial cerebrospinal fluid (ACSF; 140mM NaCl, 5mM KCl, 10mM D-glucose, 10mM HEPES, 2mM CaCl2, 2mM MgSO4, pH 7.4). V1 recordings were performed at approximately 2600 μm lateral to the sagittal suture and 600 μm anterior to the lambdoid suture.

Chronic Electrode Implantation: Mice were implanted with recording electrodes under 2% isoflurane anesthesia. These procedures were performed in two steps. First, a head plate base was placed around the implantation target area. After 7 days of recovery, mice were habituated at least 5 days to freely explore the arena (see below) with the head attached to the cables for the inertial measurement unit (IMU) and the electrophysiological recording. We also added an approximately 3g weight on the head to mimic the presence of the microdrive, the IMU, and the electrode. After this period of habituation to the setup, mice underwent the second step, namely the silicon probe implantation procedure. Just before performing the chronic electrode implantation, we sutured the eyelids of both eyes (see above). A single- or two- shank silicon probe (Cambridge NeuroTech H3 64x1 or Diagnostic Biochips P128-3, respectively) was mounted on a movable microdrive to record V1 neuronal activity. After the ground electrode implantation (0.005” diameter stainless wire, A-M systems) in the cerebellum and the craniotomy above the target implantation site, the probe

was implanted at the same stereotaxic coordinate as the acute recording. The probe was lowered to 800-900 μm below the brain's surface. After recovery from isoflurane anesthesia, the probe depth was finely adjusted by moving the microdrive so that the recording channels could sampler the entire depth of V1. The experiments were performed the day after implantation.

Bilateral Vestibular Lesions: Mice were anesthetized with 2% isoflurane and core body temperature monitored with a rectal probe and maintained at 37°C with a heating pad (FHC). The lateral regions of the posterior and horizontal semicircular canals were exposed. The canal bone was then thinned until punctured and a microfiber needle inserted to deliver kanamycin (5 μl; 50 mg/ml). The skin was sutured with a few stitches of 6/0 suture. Electrophysiological recordings in V1 were performed after mice recovered between 3 to 5 days in their home cages.

Electrophysiology—Extracellular recordings were performed using the following silicon probes Neuronexus: A1x32-5mm-25-177-A32;A1-32-Edge-5mm-20-177-A32; A2x32-5mm-25-177-A64, 1x64-Poly2-6mm-23s-160 or Cambridge Neurotech: ASSY-77 H2 (Acute 64 channel H2 probe, 2 shanks @250um, 8mm length), ASSY-77 H5 (Acute 64 channel H5 probe, 1 shank, 9 mm length). The recording electrodes were controlled with Luigs & Neumann micromanipulators and stained with DiI or DiO lipophilic dyes (Thermo Fisher) for post hoc identification of the electrode track. We recorded the signals at 30 kHz using an INTAN system (RHD2000 USB Interface Board, INTAN Technologies).

Head-fixed Rotations—To control the velocity and amplitude of head movements, we fixed the head of awake mice in the center of a servo-controlled platform enabling the rotation of the animal along the horizontal plane (50 degrees rotation; 80°/s peak velocity; unless stated otherwise Figure 1A). Mice were head-fixed, their bodies restrained in a tube, and we pseudo-randomly alternated clockwise (CW; contraversive relative to the recording site) with counterclockwise (CCW; ipsiversive) rotations. The head was positioned with a ~ 20 degrees angle along the sagittal plane of the head (nose pointing 20 degrees down), such that the plane of the horizontal vestibular canal was approximately parallel to the plane of rotating platform. The platform was attached to a gearbox 15:1 (VTR010-015-RM-71 VTR, Thomson) that increased the torque of a servo motor (AKM53L-ANC2C-00 KEC0432 AC Servomotor 1.83kW, Kolmorgen). The motor was tuned using a servo drive (AKD-B013206-NBAN-0000 servo drive, Kolmorgen) and controlled in velocity mode using analog waveforms computed in Labview.

Illumination—To illuminate the right eye homogeneously, we placed a light diffuser (DG100X100-120, Thorlabs) 3-5 cm away from the eye, and an optical fiber (core = 960 μm / NA = 0.63) coupled to a blue LED (470 nm; Doric Lenses) was placed 6-7 cm away from the diffuser. The light source, as well as the light diffuser, were attached to the rotating platform, thereby moving together with the mouse. Illuminance measured at the right eye position during the recording, was about 180 lux (R8140, Reed instruments). In the dark conditions, the illuminance level was below the threshold of most commercially available illuminance meters (threshold 0.1-1 lux). We thus measured the irradiance in the spectrum of

visible light instead (from 400 nm – 700 nm; power sensor: S130C Thorlabs), specifying the measurement wavelength at 470 nm on the digital power meter (PM100D, Thorlabs). In the dark, the irradiance was 0.15 nW/cm^2. Illumination during light trials lasted 4 s. At light onset, illumination intensity was set instantaneously to the desired power; at light offset the power was ramped down over 0.5 s to reduce rebound activity in V1. The platform started to rotate 1.22 s after light onset, reached its peak velocity 2 s after light onset, and the rotation ended 1.18 s before light offset. As light trials were randomly interleaved with dark trials, the interval between two light onsets was variable, with a minimum of 10 s. The minimal and maximal time intervals between light offset and a rotation in the dark were 6 s and 12 s, respectively.

Head-fixed rotation during continuous illumination—Mice were head-fixed on the rotating platform and both eyelids were sutured as described above. The experiment was divided into two blocks of trials. We first performed 33 to 45 trials in the dark (irradiance: 0.15 nW/cm^2; Power sensor S130C, Thorlabs; using the same parameters as in section: Illumination) followed by approximately the same number of trials in light. The illumination was provided by four computer LED monitors (Dell U2415 24-Inch 1920 x 1200 LED Monitor, 60-Hz refresh rate, gamma-corrected) mounted orthogonally to each other to form a square enclosure that covered 360° of visual field along the azimuth. The mean illuminance provided by the monitors was about 90 lux, measured at the right eye position of the mouse (R8140, Reed instruments). The two blocks of trials were separated by a transition period of 1-2 minutes.

SOM cells Photo-tagging—ChR2-expressing SOM were activated via an optical fiber (core = 960 μm/ NA = 0.63) coupled to a blue LED (470 nm; Thorlabs) and placed above V1 such as to illuminate the entire surface of V1 (Power: 5-6 mW measured at the fiber tip). LED power was measured before each experiment with a digital power meter (PM100D, Thorlabs). The photo-tagging of the cells was performed before and after the block of head rotation trials.

Freely moving animals—The mouse was placed inside a circular arena (i.e. a cylinder of 24 cm in diameter and 32 cm height made of LED light Sheet panel, TAP Plastics). The mouse carried an inertial measurement unit (IMU) on its head placed parallel to the sagittal suture axis. Recording electrodes were connected to an assisted electrical rotary joint commutator (AERJ_12_HARW, Doric) with a RHD2000 0.9m ultra-thin SPI cable (INTAN, Part #C3213) using an omnetics adapter (ADAPTER_HO12, Doric). The IMU cable passed through the motorized commutator and connected to a non-motorized commutator (Slip ring Flange - 22mm diameter, Adafruit) that was placed on top of the motorized one. As both cables were attached together, the motorized commutator triggered the rotation of both cables together to compensate for head motion. The inertial signal was sent to a DAQ card and data were acquired using a Labview software, whereas electrophysiological signals were sent to the INTAN board. Homogeneous illumination of the arena was obtained using an LED strip (Ustelar) attached to the wall of a cylinder (40 cm diameter) surrounding the wall of the arena. Sequences of 2 minutes light (about 170 lux at the center of the arena) and dark (irradiance: 0.16 nW/cm^2) were alternated randomly, controlled via Labview.

Tracking head movements in freely moving animals—The IMU (see section Freely moving animals, above) detected linear acceleration and angular velocity. The movement sensor board was built around the TDK/Invensense MPU-9x50 9 axis movement sensor (Pasquet et al., 2016). The movement sensor USB interface supplied the sensor power, configuration, and data acquisition. Angular velocity data were acquired at 300Hz. The USB interface sent a synchronization input used to timestamp the electrophysiological recording by sending a signal to the INTAN board.

Monitoring eye movements by video-oculography—The movement of the right eye was monitored through a high-speed infrared (IR) camera (Imperx Bobcat, B0620). The camera captured the reflection of the eye on an IR mirror (transparent to visible light, Edmund Optics #64–471) under the control of custom Labview software and a frame grabber (National Instrument PCIe-1427). The pupil was identified online by thresholding pixel values or *post hoc* by combining thresholding and morphology operation and its profile was fitted with an ellipse to determine the center. The eye position was measured by computing the distance between the pupil center and the corneal reflection of a reference IR LED placed along the optical axis of the camera. To calibrate the measurement of the eye position, the camera and the reference IR LED were moved along a circumference centered on the image of the eye by ± 10° (Liu et al., 2016).

Histology—For anatomical analysis, mice were transcardially perfused with phosphate buffered saline (PBS) and then with 4% paraformaldehyde (PFA) in PBS. Brains were extracted from the skulls, post-fixed in 4% PFA overnight at 4°C, and subsequently cut with a vibratome to 80-100 μm thick sequential coronal sections. Slices were collected and mounted in ProLong Gold (Life Technologies) or Vectashield mounting medium containing DAPI (Vector Laboratories H1500). Bright-field and fluorescence images were acquired using an Olympus MVX10 MacroView microscope. For quantification of the cell-specific ablation induced with caspase-3 virus injection in V1 (see sections: Viruses and Viral Injections), cells were counted for every mouse over a distance of 800 μm mediolateral and 400 μm anteroposterior relative to the recording site. The number of cells in ablated areas was compared to the non-ablated right hemisphere from the same animals. For PV cell ablation, cells were counted for every mouse over a distance of 400 μm mediolateral and 400 μm anteroposterior relative to the recording site.

QUANTIFICATION AND STATISTICAL ANALYSIS

Data Analysis

Unit isolation: Automated spike sorting was carried out using KiloSort (https://github.com/cortex-lab/Kilosort) by manual curation of the units using Phy (http://phycontrib.readthedocs.io/en/latest/template-gui/). Single units were identified, and all the following analysis was carried out via Matlab (MathWorks). We excluded units with refractory period violations greater than 1%.

Response to platform rotations and vestibular modulation index (vMI): The baseline spike rate was calculated on individual trials by averaging the spike rate over a window of 580 ms recorded when the platform was stationary before the rotation. The spike rate in

response to the rotation of the platform was calculated on the same trials by averaging the spike rate over a window of 580 ms centered around the peak of the rotation velocity profile. Wilcoxon signed-rank tests were then applied to determine if a cell was significantly modulated ($P<0.05$) by the rotation of the platform. We computed the vestibular modulation index as follow, vMI = (head rotation FR − head stationary FR) / (head rotation FR + head stationary FR) using the same time window as specified above. To compare the vMI collected from 2 populations of mice, we performed Wilcoxon rank sum tests. When reporting average vMIs, all cells were included, regardless of whether they were significantly modulated by the vestibular stimulus. Wilcoxon signed rank tests were performed to compare values obtained in the same recording (i.e. comparing dark and light conditions).

Response to light and luminance modulation index (lumMI): The spike rate before light onset was calculated on individual trials by averaging the spike rate over a time window of 500 ms just before the onset of the light. The spike after light onset was calculated on the same trials by averaging the spike rate over a 500 ms window beginning 500 ms after light onset. Wilcoxon signed-rank tests were then applied to determine if a cell was significantly modulated ($P<0.05$) by light. We computed the luminance modulation index as follow, lumMI = (FR in light − FR in dark) / (FR in light + FR in dark) using the same time window as specified above. To compare the lumMI collected from 2 populations of mice, we performed Wilcoxon rank sum tests. When reporting average lumMIs, all cells were included, regardless of whether or not they were significantly modulated by light.

Direction Preference Index: We define the direction preference index as (Rcw − Rccw) / (Rcw + Rccw), where Rcw and Rccw are the response of individual cells to clockwise and counterclockwise rotations, respectively (Figure S3E).

Definition of RS and FS cells: Cells were classified as fast or regular spiking based on properties of their average waveforms, at the electrode site with largest amplitude (Niell and Stryker, 2008). Briefly, three parameters were used for discrimination: the height of the positive peak relative to the initial negative trough, the time from the minimum of the initial trough to maximum of the following peak, and the slope of the waveform 0.5 ms after the initial trough. Two separable clusters were found, corresponding to fast-spiking (putative inhibitory) and regular-spiking (putative excitatory) neurons. These clusters were separated using a k-means clustering method. The same analysis was performed for both head fixed and freely moving recordings.

SOM cells analysis: Cells were considered to be putative SOM cells when their activity during the blue LED illumination of V1 triggered a significant increase of firing rate within the first 6 ms illumination ($P<0.05$, Wilcoxon signed rank test). For our analysis, we included only SOM cells with regular spike shape (see section: Definition of RS and FS cells). We excluded from our analysis five putative SOM cells that had fast spiking shape because they are non-Martinotti cells (Ma et al., 2006; Naka et al., 2019; Nigro et al., 2018).

Head rotation modulation index in freely moving animals: Spikes from isolated units were binned at the acquisition frequency of the IMU system (300Hz, see section: Tracking

head movements in freely moving animals) to obtain the number of spikes for each angular velocity value. We computed the head rotation modulation index in freely moving mice as follow, hrMI = (head rotation FR − head stationary FR) / (head rotation FR + head stationary FR). Head rotation FR is the average firing rate between 70-90°/s (a velocity comparable to what has been used in head-fixed condition, i.e. 80°/s, see above). Stationary FR is the firing rate at 0°/s). To test the significance of the hrMI, we shuffled the spikes, computed the hrMI for 1000 randomizations and calculated the mean value m and standard deviation σ of obtained distribution of hrMIs. The statistical P-value of the hrMI measured in the experimental data set was computed as 1-F(hrMI, m, σ), where F is the cumulative Gaussian distribution with average m and standard deviation σ. Both fast spiking and regular spiking cells were merged together.

Cortical depth estimation: Cortical depth from pia estimated by using electrophysiological landmarks across layers. Average current source density (CSD) map and LFP traces during light flashes allowed us to locate layer 4 in V1 (Niell and Stryker, 2008). Moreover, the Multi-unit (MUA) spectral power (500 Hz to 5 kHz) distribution along the probe track allowed us to locate layer 5a (Senzai et al., 2019). Together, these two properties allowed us to normalize the cortical depth from the pia across mice.

Statistics—Statistical analyses were done using Matlab. No statistical tests were used to predetermine sample size, but our sample sizes are similar to those generally employed in the field. All data are presented as mean ± standard error of the mean (SEM), unless otherwise noted. The stated P-values are the results of the non-parametric Wilcoxon rank sum test to compare values between different mice or recordings, and the non-parametric Wilcoxon signed rank test to compare values from the same recording in different experimental conditions. Experiments and analyses were not blinded.

Supplementary Material

Refer to Web version on PubMed Central for supplementary material.

Acknowledgments

We thank all the members of the Scanziani and the Nelson lab for discussions about the project and comments on the manuscript; A. Nelson, R. Nicoll , B. Barbour, S. Dieudonné, N. Rebola, and B. Liu for critical reading of the manuscript; and M. Mukundan, J. Lee, B. Wong, L. Bao, Y. Li, and O. Lahrach for technical support.

Funding

This project was supported by the Howard Hughes Medical Institute and the NIH (R01EY025668) and, the JSPS (Japan Society for the Promotion of Science) for Y.S.

Bibliography

Akerman CJ, Smyth D, and Thompson ID (2002). Visual experience before eye-opening and the development of the retinogeniculate pathway. Neuron. 36, 869–879. [PubMed: 12467590]

Angelaki DE (2004). Eyes on target: What neurons must do for the vestibuloocular reflex during linear motion. J. Neurophysiol 92, 20–35. [PubMed: 15212435]

Angelaki DE, and Cullen KE (2008). Vestibular System: The Many Facets of a Multimodal Sense. Annu. Rev. Neurosci 31, 125–150. [PubMed: 18338968]

Bense S, Stephan T, Yousry TA, Brandt T, and Dieterich M (2001). Multisensory cortical signal increases and decreases during vestibular galvanic stimulation (fMRI). J. Neurophysiol 85, 886–899. [PubMed: 11160520]

Bortone DS, Olsen SR, and Scanziani M (2014). Translaminar inhibitory cells recruited by layer 6 corticothalamic neurons suppress visual cortex. Neuron 82, 474–485. [PubMed: 24656931]

Bremmer F, Klam F, Duhamel JR, Ben Hamed S, and Graf W (2002). Visual-vestibular interactive responses in the macaque ventral intraparietal area (VIP). Eur. J. Neurosci 16, 1569–1586. [PubMed: 12405971]

Duffy CJ (1998). MST neurons respond to optic how and translational movement. J. Neurophysiol 80, 1816–1827. [PubMed: 9772241]

Gu Y, Watkins PV, Angelaki DE, and DeAngelis GC (2006). Visual and nonvisual contributions to three-dimensional heading selectivity in the medial superior temporal area. J. Neurosci 26, 73–85. [PubMed: 16399674]

Guitchounts G, Masis J, Wolf SB, and Cox D (2020). Encoding of 3D Head Orienting Movements in Primary Visual Cortex. BiorXiv. 2020.01.16.909473.

Iurilli G, Ghezzi D, Olcese U, Lassi G, Nazzaro C, Tonini R, Tucci V, Benfenati F, and Medini P (2012). Sound-Driven Synaptic Inhibition in Primary Visual Cortex. Neuron 73, 814–828. [PubMed: 22365553]

Ji XY, Zingg B, Mesik L, Xiao Z, Zhang LI, and Tao HW (2016). Thalamocortical Innervation Pattern in Mouse Auditory and Visual Cortex: Laminar and Cell-Type Specificity. Cereb. Cortex 26, 2612–2625. [PubMed: 25979090]

Jun JJ, Steinmetz NA, Siegle JH, Denman DJ, Bauza M, Barbarits B, Lee AK, Anastassiou CA, Andrei A, Aydin C et al. (2017). Fully integrated silicon probes for high-density recording of neural activity. Nature 551,232–236. [PubMed: 29120427]

Kayama Y, Riso RR, Bartlett JR, and Doty RW (1979). Luxotonic responses of units in macaque striate cortex. J. Neurophysiol 42, 1495–1517. [PubMed: 115968]

Kinoshita M, and Komatsu H (2001). Neural representation of the luminance and brightness of a uniform surface in the macaque primary visual cortex. J. Neurophysiol 86, 2559–2570. [PubMed: 11698542]

Krug K, Akerman CJ, and Thompson ID (2001). Responses of neurons in neonatal cortex and thalamus to patterned visual stimulation through the naturally closed lids. J. Neurophysiol 85, 1436–1443. [PubMed: 11287467]

Lee SH, Hjerling-Leffler J, Zagha E, Fishell G, and Rudy B (2010). The largest group of superficial neocortical GABAergic interneurons expresses ionotropic serotonin receptors. J. Neurosci 30, 16796–16808. [PubMed: 21159951]

Leinweber M, Ward DR, Sobczak JM, Attinger A, and Keller GB (2017). A Sensorimotor Circuit in Mouse Cortex for Visual Flow Predictions. Neuron 95, 1420–1432. [PubMed: 28910624]

Lima SQ, Hromádka T, Znamenskiy P, and Zador AM (2009). PINP: A new method of tagging neuronal populations for identification during in vivo electrophysiological recording. PLoS One 4(7): e6099. [PubMed: 19584920]

Liu BH, Huberman AD, Scanziani M (2016). Cortico-fugal output from visual cortex promotes plasticity of innate motor behaviour. Nature. 2016; 538: 383–387 [PubMed: 27732573]

Ma Y, Hu H, Berrebi AS, Mathers PH, and Agmon A (2006). Distinct subtypes of somatostatin-containing neocortical interneurons revealed in transgenic mice. J. Neurosci 26, 5069–5082. [PubMed: 16687498]

Macé É, Montaldo G, Trenholm S, Cowan C, Brignall A, Urban A, Roska B (2018) Whole-brain functional ultrasound imaging reveals brain modules for visuomotor integration. Neuron 100, 1241–1251. [PubMed: 30521779]

Vanni-Mercier G, and Magnin M (1982). Single Neuron Activity Related to Natural Vestibular Stimulation in the Cat's Visual Cortex. Exp. Brain Res 45(3):451–455. [PubMed: 7067779]

Naka A, Veit J, Shababo B, Chance RK, Risso D, Stafford D, Snyder B, Egladyous A, Chu D, Sridharan S, Mossing DP, Paninsky L, Ngai J, and Adesnik H (2019). Complementary networks of cortical somatostatin interneurons enforce layer specific control. eLife 2019;8:e43696 [PubMed: 30883329]

Niell CM, and Stryker MP (2008). Highly selective receptive fields in mouse visual cortex. J. Neurosci. 28, 7520–7536. [PubMed: 18650330]

Nigro MJ, Hashikawa-Yamasaki Y, and Rudy B (2018). Diversity and connectivity of layer 5 somatostatin-expressing interneurons in the mouse barrel cortex. J. Neurosci 38, 1622–1633. [PubMed: 29326172]

Ohshiro T, Angelaki DE, and DeAngelis GC (2017). A Neural Signature of Divisive Normalization at the Level of Multisensory Integration in Primate Cortex. Neuron 95, 399–411. [PubMed: 28728025]

Pasquet MO, Tihy M, Gourgeon A, Pompili MN, Godsil BP, Léna C, and Dugué GP (2016). Wireless inertial measurement of head kinematics in freely-moving rats. Sci. Rep 6, 1–13. [PubMed: 28442746]

Pfeffer CK, Xue M, He M, Huang ZJ, and Scanziani M (2013). Inhibition of inhibition in visual cortex: the logic of connections between molecularly distinct interneurons. Nat. Neurosci 16, 1068–1076. [PubMed: 23817549]

Rancz EA, Moya J, Drawitsch F, Brichta AM, Canals S, and Margrie TW (2015). Widespread vestibular activation of the rodent cortex. J. Neurosci 35, 5926–5934. [PubMed: 25878265]

Senzai Y, Fernandez-Ruiz A, and Buzsáki G (2019). Layer-Specific Physiological Features and Interlaminar Interactions in the Primary Visual Cortex of the Mouse. Neuron 101, 500–513. [PubMed: 30635232]

Storchi R, Bedford RA, Martial FP, Allen AE, Wynne J, Montemurro MA, Petersen RS, and Lucas RJ (2017). Modulation of Fast Narrowband Oscillations in the Mouse Retina and dLGN According to Background Light Intensity. Neuron 93, 299–307. [PubMed: 28103478]

Takahashi K, Gu Y, May PJ, Newlands SD, DeAngelis GC, and Angelaki DE (2007). Multimodal coding of three-dimensional rotation and translation in area MSTd: comparison of visual and vestibular selectivity. J. Neurosci 27, 9742–9756. [PubMed: 17804635]

Thomas D, Harrell ER, Kempf A, Ceballo S, Filipchuk A, and Bathellier B (2019) Context-dependent signaling of coincident auditory and visual events in primary visual cortex. eLife 2019;8:e44006 [PubMed: 31115334]

Tucker TR, and Fitzpatrick D (2006). Luminance-Evoked Inhibition in Primary Visual Cortex: A Transient Veto of Simultaneous and Ongoing Response. J. Neurosci 26, 13537–13547. [PubMed: 17192437]

Vélez-Fort M, Bracey EF, Keshavarzi S, Rousseau CV, Cossell L, Lenzi SC, Strom M, and Margrie TW (2018). A Circuit for Integration of Head- and Visual-Motion Signals in Layer 6 of Mouse Primary Visual Cortex. Neuron 93, 179–191.

Wang Q, and Burkhalter A (2007). Area map of mouse visual cortex. J. Comp. Neurol 502, 339–357. [PubMed: 17366604]

Wenzel R, Bartenstein P, Dieterich M, Danek A, Weindl A, Minoshima S, Ziegler S, Schwaiger M, and Brandt T (1996). Deactivation of human visual cortex during involuntary ocular oscillations A PET activation study. Brain 119, 101–110. [PubMed: 8624674]

Xing D, Yeh C-I, Gordon J, and Shapley RM (2014). Cortical brightness adaptation when darkness and brightness produce different dynamical states in the visual cortex. Proc. Natl. Acad. Sci 111, 1210–1215. [PubMed: 24398523]

Highlights

- Head movements in darkness suppress V1 activity.
- Head movements in light increase V1 activity.
- Specific inhibitory neurons mediate V1 suppression by head movements in darkness.

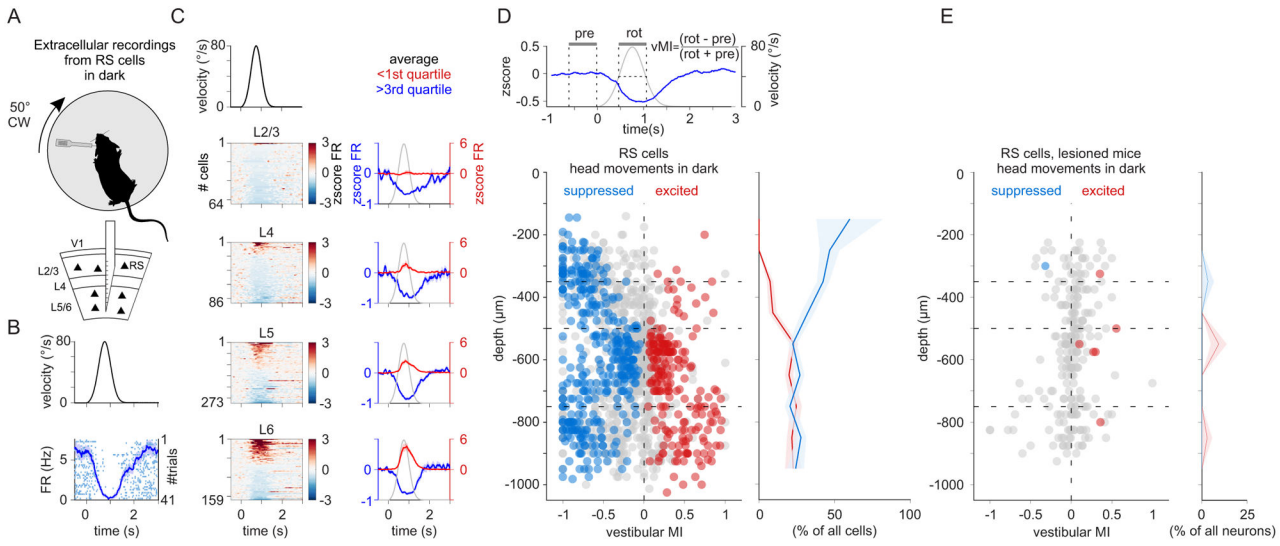

Figure 1. Suppression of V1 by head movements in dark

(A) Experimental configuration: Top: An extracellular linear probe in the left primary visual cortex (V1) of a head-fixed, awake mouse records the response to clockwise (CW) rotations of the table in dark. Bottom: The linear probe spanned all cortical layers. RS: regular spiking cell.

(B) Top: Velocity profile of the rotating table (CW rotation). Bottom: Example RS cell located 550 µm below the pial surface. Raster plot and averaged peristimulus time histogram (PSTH) are superimposed.

(C) Summary of 582 significantly modulated RS cells subdivided according to cortical depth (from the pia). Left panels: Velocity profile of the rotating table (CW rotation; top panel) and heat maps of the z-score of the firing rate (zscore FR) of individual RS cells during rotations of the table. Within each panel, cells are sorted by the peak z-score. Right panels: Blue and red traces are the average z-scores of all cells whose z-score was smaller or larger than the first or third quartile, respectively. The gray trace is the velocity profile of the table (CW rotation).

(D) Top left: The time windows used to compute the vestibular modulation index (vMI; blue trace: average of all significantly suppressed RS cells; gray trace: velocity profile). Bottom left: vMI for CW rotations of individual RS cells plotted against cortical depth. Blue, red, and gray circles are suppressed, excited, and non-significantly modulated RS cells, respectively (superficial layers vMI: −0.45±0.02; n = 353 cells; Deep layers vMI: −0.15±0.01; n = 978 cells; 36 recordings from 30 mice). Horizontal dotted lines indicate approximate layer borders. Right: Percentage of significantly suppressed (blue) and excited (red) RS cells plotted against cortical depth (superficial layers: 32±4% suppressed; 6±1% excited, Deep layers: 25±2% suppressed; 22±2% excited).

(E) As (D) but for vestibular lesioned mice (2.7% of RS cells modulated by rotation, 7 out of 253 cells, n = 3 mice).

Shading is SEM.

Related to Figure S1 and S2A-D.

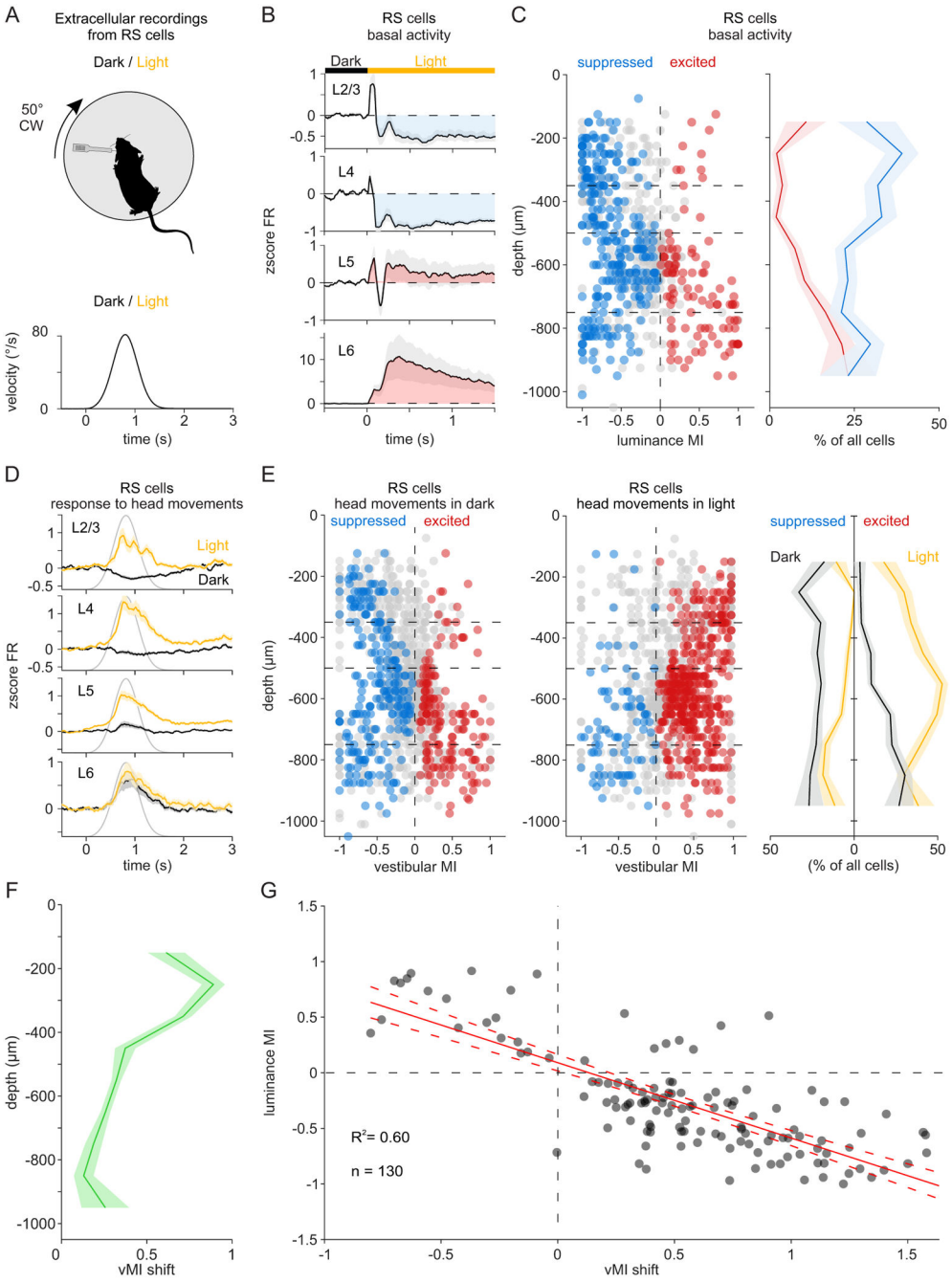

Figure 2. Excitation of V1 by head movements in light

(A) Experimental configuration: Top: As in Figure 1A but rotations are alternated between dark and light. Bottom: Velocity profile of the rotation.

(B) Averaged z-score of the firing rate (zscore FR) of RS cells in response to light onset. Each average is contributed by all the cells recorded within the layer indicated in the panel, independently of whether they were excited, suppressed, or non-significantly modulated by light onset. Blue or red shaded area indicate average suppression or excitation by light, respectively. Horizontal colored bar indicates time of dark/light transition (time 0).

(C) Luminance modulation index (lumMI) of individual RS cells plotted against cortical depth. Superficial layers lumMI: −0.58±0.02; Deep layers lumMI: 0.17±0.018. Right: percentage of suppressed (blue) and excited (red) RS cells plotted against cortical depth in response to light onset.
(D) zscore FR of RS cells during CW rotations in dark (black traces) and in light (yellow traces). Each average is contributed by all the cells recorded within the layer indicated in the panel, independently of whether they were excited, suppressed, or non-significantly modulated by the rotation. Gray trace is velocity profile.
(E) Vestibular modulation index (vMI) for CW rotations of individual RS cells plotted against cortical depth. Same cells as in C. Left: vMI of RS cells in dark; Middle, vMI of the same RS cells in light. For RS cells recorded in superficial layers, the vMI shifted from −0.30±0.02 in dark to 0.36±0.03 in light (P = 6.1e-43; n = 373 cells). In deep layers, the vMI of RS cells shifted from −0.08±0.016 in dark to 0.17±0.02 in light (P = 1.5e-33; n = 701 cells, 18 recordings from 12 mice). Right: percentage of suppressed and excited RS cells plotted against cortical depth in dark (black) and light (yellow). Note the shift towards positive vMI in light.
(F) vMI shift (vMI in light - vMI in dark) plotted against the cortical depth. Positive vMI shift indicate facilitation of the response to head movements in light as compared to dark.
(G) vMI shift plotted against lumMI. Only RS cells with a significant lumMI and a significant vMI shift (n = 130 cells) are included. Continuous red line: linear regression (R^2 = 0.60). Dotted red lines: confidence interval of linear regression.
Horizontal dotted lines indicate approximate layer borders for (C) and (E).
Blue, red, and gray circles are suppressed, excited, and non-significantly modulated RS cells, respectively for lumMI in (C) and vMI in (E).
Shading is SEM.
Related to Figure S2E-K, S3, and S4.

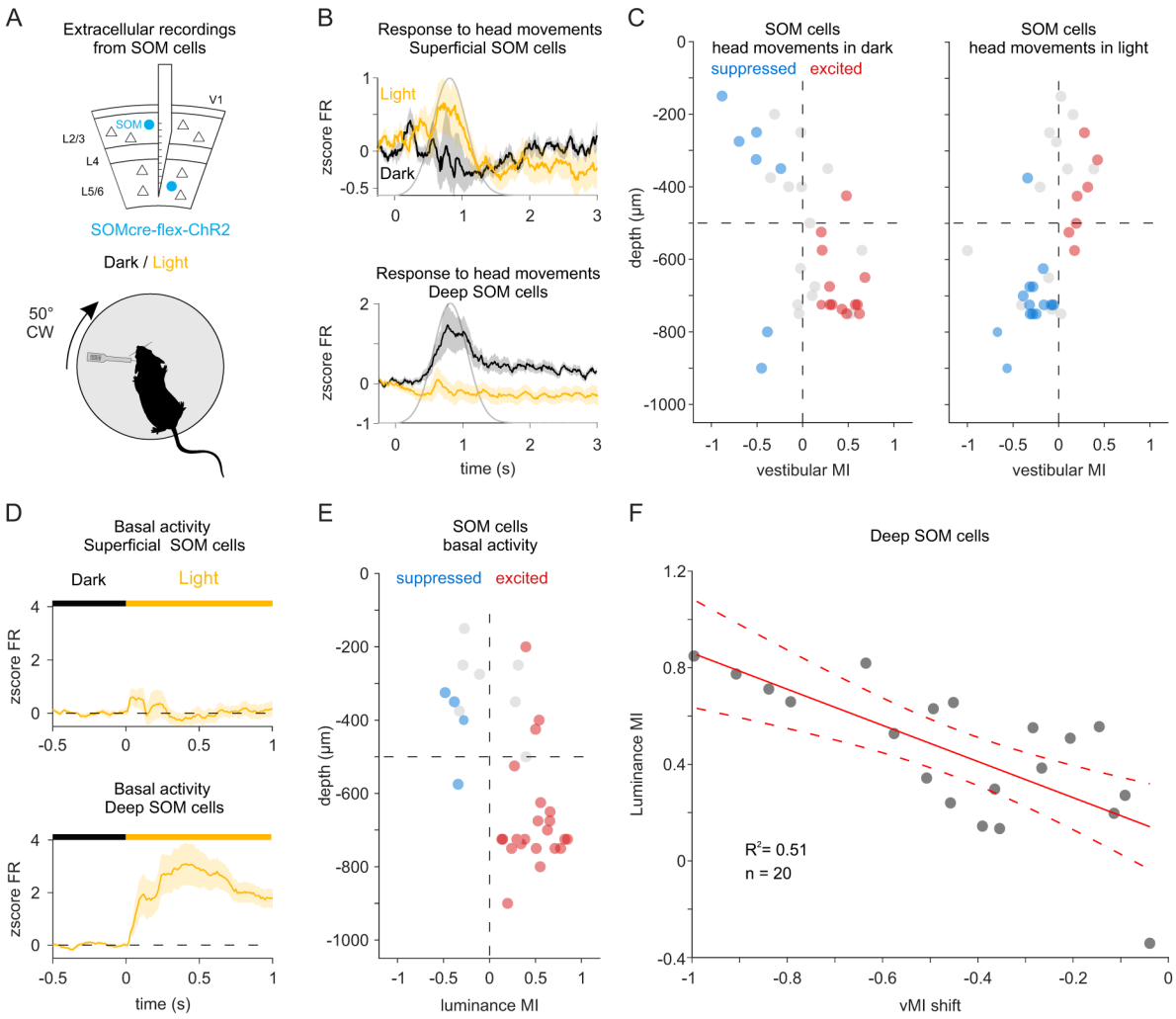

Figure 3. Excitation of layer 5 SOM cells by head movements in dark and suppression in light

(A) Experimental configuration. Schematic of extracellular recordings from photo-tagged SOM cells in V1 (top) of a head-fixed, awake mouse in response to clockwise (CW) rotation of the table, in dark and light (bottom).

(B) Averaged z-score of the firing rate (zscore FR) of SOM cells during CW rotations in dark (black traces) and in light (yellow traces) for SOM cells recorded in the superficial layers (top panel; n = 12) and deep layers (bottom panel; n = 20). Gray trace is velocity profile.

(C) Vestibular modulation index (vMI) to CW rotations of individual SOM cells plotted against cortical depth. Left: vMI of SOM cells in dark; Right, vMI of the same SOM cells in light (Dark vs Light : Superficial layers vMI: −0.24±0.11 vs 0.10±0.07; P = 0.021; Deep layers vMI: 0.25±0.07 vs −0.23±0.06; P = 6.1e-5; n= 32 SOM cells; 15 recordings from 8 mice). Note shift of deep layer SOM cells towards negative vMIs.

(D) zscore FR of SOM cells in response to light onset for SOM cells recorded in the superficial layers (top panel; n = 12) and deep layers (bottom panel; n = 20). Horizontal colored bar indicates time of dark/light transition (time 0). Note the strong increase in firing rate of deep layer SOM cells by light.

(E) Luminance modulation index of SOM cells plotted against cortical depth (Superficial layers lumMI: - 0.009±0.11; Deep layers lumMI: 0.44±0.06, same cells as in C).
(F) vMI shift (vMI in light - vMI in dark) plotted against lumMI. Continuous red line: linear regression (R^2 = 0.51; n = 20). Dotted red lines: confidence interval of the linear regression. Note negative values of vMI shift as compared to RS cells (Figure 2G) yet similar inverse relationship between vMI shift and lumMI.
Horizontal dotted line indicates approximate border between superficial and deep layers (between layer 4 and 5) for (B) and (E).
Blue, red, and gray circles are suppressed, excited, and non-significantly modulated SOM cells, respectively for lumMI in (C) and vMI in (E).
Shading is SEM.

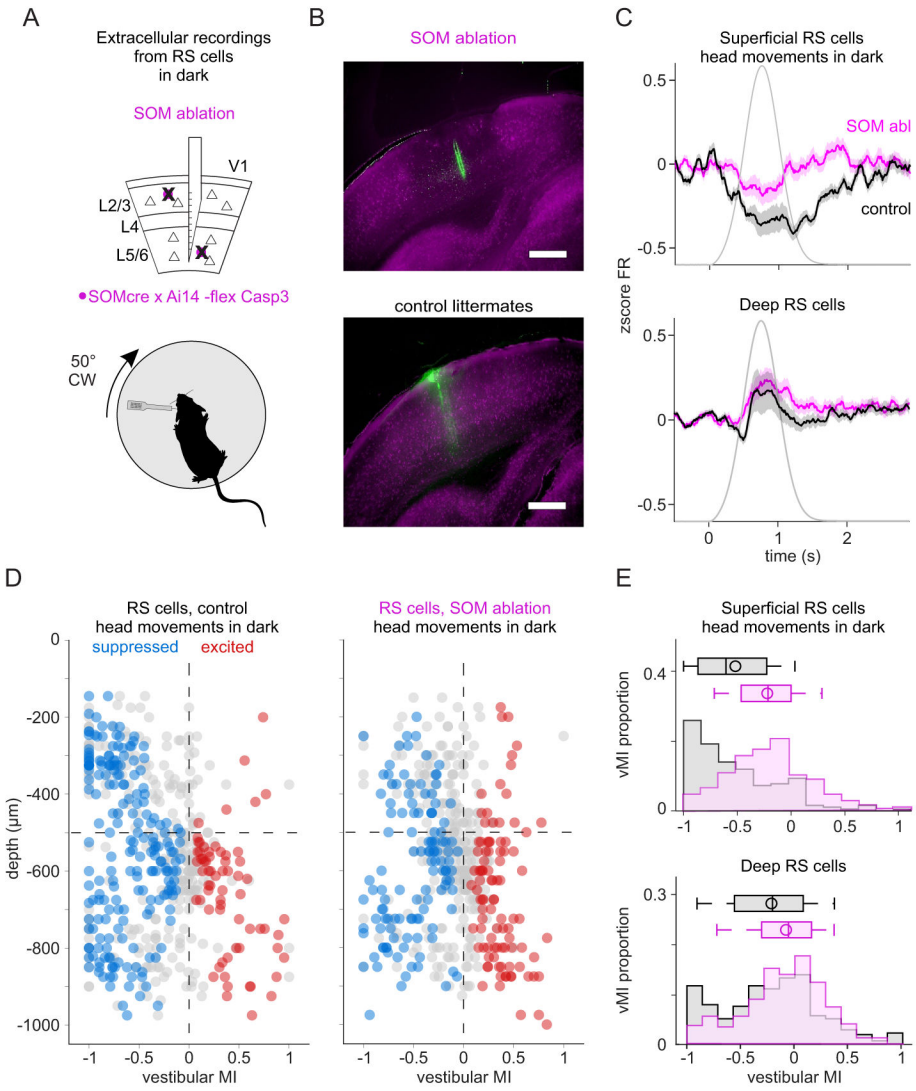

Figure 4. SOM cells suppress V1 in response to head movements in dark

(A) Experimental configuration: Schematic of a linear probe in V1 in which SOM cells have been ablated (top) to record the activity of RS cells in a head-fixed, awake mouse in response to clockwise (CW) rotation of the table in the dark (bottom).

(B) Fluorescence microscopy images of V1 coronal sections (SOM Cre x Ai14 mouse) with (top panel) or without (bottom panel) the conditional expression of virally injected caspase-3. The electrode track is in green. Scale bar: 400 µm.

(C) Averaged z-score of the firing rate (zscore FR) of RS cells during CW rotations in dark for SOM ablated mice (magenta) and un-injected, control littermates (black). Top panel: All RS cells recorded in superficial layers (n = 149 cells (magenta) and 182 cells (black)). Bottom panel: All RS cells recorded in deep layers (n = 339 cells (magenta) and 333 cells (black)). Shading is SEM. Gray trace is velocity profile.

(D) Vestibular modulation index (vMI) for CW rotations of individual RS cells plotted against cortical depth. Blue, red, and gray circles are suppressed, excited, and non-significantly modulated RS cells, respectively. Left: vMI of RS cells in non-injected

littermates. Right: vMI of RS cells in SOM ablated mice (Control (n=11 mice) vs Ablation (n=9 mice), Superficial layers vMI: −0.56±0.03 (n = 182 cells) vs −0.20±0.03 (n = 149 cells), P = 3.2e-16; suppressed: 38±3% vs 25±4%, P = 0.027; excited: 4.8±1.4% vs 19±3%, P = 0.0023; Deep layers vMI: −0.22±0.025 (n = 333 cells) vs −0.073±0.02 (n = 339 cells), P = 3.1e-6; suppressed: 32±2% vs 21±1%, P = 0.001; excited: 19±3% vs 27±2%, P = 0.044; 1 recording per mouse for both conditions). Horizontal dotted line indicates approximate border between superficial and deep layers (between layer 4 and 5). Note shift towards positive vMI in SOM ablated animals, especially in superficial layers.

(E) Distribution of the vMI in SOM ablated mice (magenta) and control littermates (black) for RS cells recorded in superficial (top panel) and deep (bottom panel) layers. Box plots show median, first and third quartiles, minimum/maximum values and mean (circle). Related to Figure S5 and S6

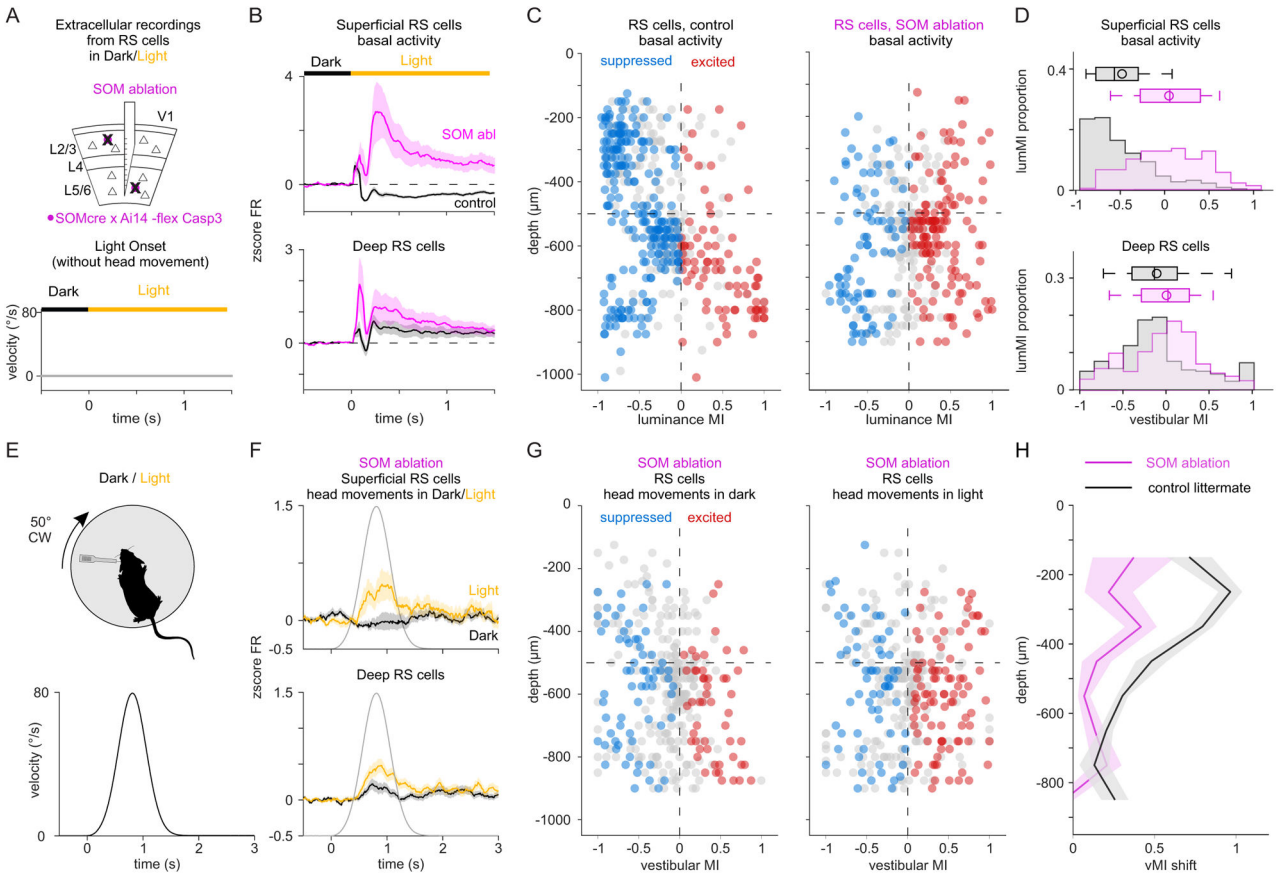

Figure 5. SOM cells contribute to light-mediated facilitation of V1 response to head movements

(A) Experimental configuration: Schematic of a linear probe in V1 in which SOM cells have been ablated (top) to record the activity of RS cells in a head-fixed, awake mouse in response to light onset (without head movement; bottom).

(B) Averaged z-score of the firing rate (zscore FR) of RS cells in response to light onset in SOM ablated mice (magenta) and control littermates (black). Top panel: All RS cells recorded in superficial layers (n = 99 cells (magenta) and 199 cells (black)). Bottom panel: All RS cells recorded in deep layers (n = 260 cells (magenta) and 276 cells (black)). Horizontal colored bar indicates time of dark/light transition (time 0).

(C) Luminance modulation index (lumMI) of individual RS cells plotted against cortical depth. Left: lumMI of RS cells in un-injected littermates; Right: lumMI of SOM ablated mice (Control (n=8 mice) vs SOM ablation (n=8 mice): Superficial layers lumMI: −0.50±0.03 (n = 199 cells) vs 0.04±0.05 (n = 99 cells); P = 8.5e-20; suppressed: 60±10% vs 25±6%, P = 0.015; excited: 4.6±1.6% vs 41±10%, P = 0.005; Deep layers lumMI: -0.09±0.03 (n = 270 cells) vs −0.01±0.03 (n = 260 cells), P = 0.003; suppressed: 42±8% vs 27±4%, P = 0.05; excited: 15±4% vs 41±5%, P = 0.002, 1 recording per animal). Note shift towards positive lumMI in SOM ablated mice.

(D) Distribution of the lumMI in SOM ablated mice (magenta) and control littermates (black) for RS recorded in superficial (top panel) and deep (bottom panel) layers. Box plots show median, first and third quartiles, minimum/maximum values and mean (circle).

(E) Experimental configuration: Top: The extracellular linear probe is inserted in the left V1 of the head-fixed, awake mouse to record the activity of RS cells in SOM ablated mice in response to clockwise (CW) rotation of the table in dark and light. Bottom: Velocity profile of the rotating table (CW rotation).

(F) zscore FR of RS cells recorded in SOM ablated mice during CW rotations in dark (black) and light (yellow). Top panel: All RS cells recorded in superficial layers (n = 99 cells, magenta). Bottom panel: All RS cells recorded in deep layers (n = 260 cells, black). Gray trace is velocity profile.

(G) Vestibular modulation index (vMI) for CW rotations of individual RS cells recorded in SOM ablated mice plotted against cortical depth. vMI of RS cells in dark (left) and light (right; n = 359 RS cells; 8 mice; 1 recording per mouse). Note reduced shift of vMI in SOM ablated mice as compared to control (Fig 2E) and as compared to un-injected littermates (data not shown).

(H) vMI shift (vMI in light - vMI in dark) plotted against cortical depth. Magenta: SOM ablated mice. Control littermates vs SOM ablation: vMI shift in superficial layers: 0.79±0.04 vs 0.26±0.06, P = 7.2e-13; vMI shift in deep layers: 0.25±0.03 vs 0.08±0.03, P = 8.0e-7; data not shown for the littermates). Note the reduction in vMI shift in SOM ablated mice as compared to control littermates (black line).

Horizontal dotted line indicates approximate border between superficial and deep layers (between layer 4 and 5) for (C) and (F).

Blue, red, and gray circles are suppressed, excited, and non-significantly modulated RS cells, respectively, for (C) and (G)

Shading is SEM.

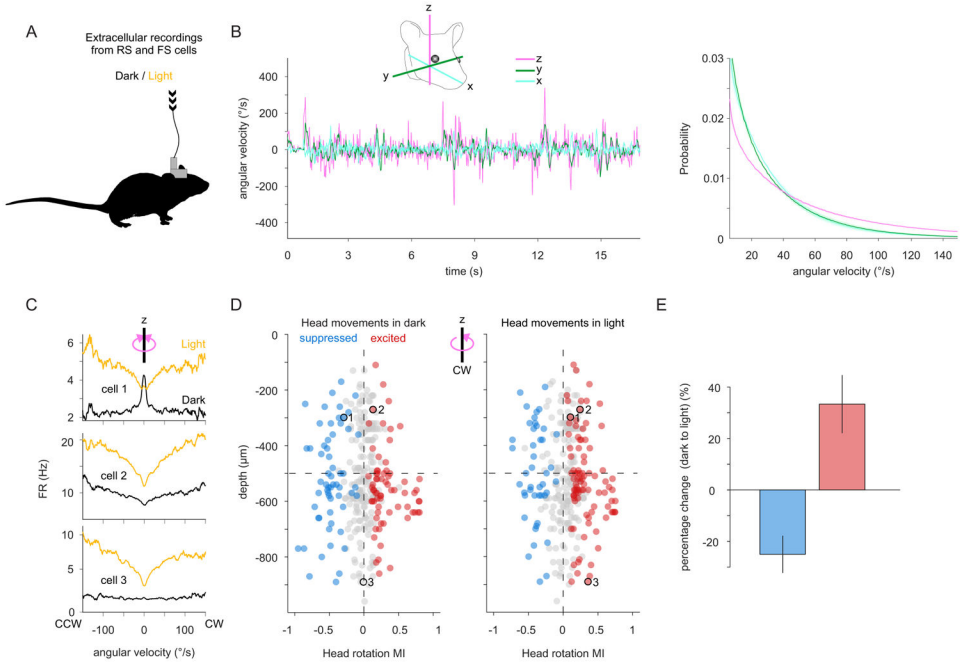

Figure 6. Light mediated facilitation of V1 activity to head movements in freely moving mice

(A) Experimental design: A chronic extracellular linear probe is inserted in V1 of a freely moving mouse. Head motion is monitored with an IMU attached to the head. Light and dark condition are alternated every 2 minutes.

(B) Left: Example traces illustrating head angular velocity in time around 3 orthogonal axes of rotation. Inset: Schematic illustration of the three axes relative to the head of the mouse. Right: Probability distribution of angular velocity around the three axes of rotation. Shading is SEM.

(C) Firing rate (FR) plotted against angular velocity around the z-axis (yaw) for 3 example cells in dark (black traces) and in light (yellow traces). Positive and negative values are clockwise (CW) and counterclockwise (CCW) rotations, respectively. Note that Cell 1 is suppressed by yaw in dark and excited by yaw in light, Cell 2 is more excited by yaw in light than in dark, and Cell 3 does not respond to yaw in dark but is excited by yaw in light.

(D) Head rotation modulation index (hrMI) for CW rotations of individual isolated cells plotted against cortical depth. Blue, red, and gray circles are suppressed, excited, and non-significantly modulated cells, respectively. Left: hrMI of isolated cells in dark; Left, hrMI of the same cells in light (n = 324 cells; 4 recordings from 4 mice). Black circles illustrate examples cells from (C). Horizontal dotted line indicates 500 µm depth. Note shift towards positive hrMI in light. Cortical depth is measured from the pia.

(E) Change in the percentage of suppressed (blue) and excited (red) cells in response to CW head rotations around the z-axis from dark to light. Note the decrease in suppressed (−25±8%) and the increase in exited cells (33.3±11.8%). Percentages are mean ± SEM.

KEY RESOURCES TABLE

REAGENT or RESOURCE	SOURCE	IDENTIFIER
Bacterial and Virus Strains		
AAV1-EF1a-flex-taCasp3-TEVp	Univ. of North Carolina Viral Vector Core	N/A
AAV1-EF1a-DIO-hChR2(H134R)-EYFP	Univ. of Pennsylvania Viral Vector Core	N/A
Chemicals, Peptides, and Recombinant Proteins		
DiI	Thermo Fisher	Cat#22885
Vectashield-Hardset	Vector Laboratories, H1500	RRID:AB_2336788
Experimental Models: Organisms/Strains		
Mouse: B6J.Cg-Sst$^{tm2.1(cre)Zjh}$/MwarJ	The Jackson Laboratory	RRID:IMSR_JAX:028864
Mouse: B6.Cg-Gt(ROSA)26Sor$^{tm32(CAG-COP4*H134R/EYFP)Hze}$/J	The Jackson Laboratory	RRID:IMSR_JAX:024109
Mouse: B6.Cg-Gt(ROSA)26Sor$^{tm14(CAG-tdTomato)Hze}$/J	The Jackson Laboratory	RRID:IMSR_JAX:007914
Mouse: B6.129P2-Pvalb$^{tm1(cre)Arbr}$/J	The Jackson Laboratory	RRID:IMSR_JAX:017320
Mouse: STOCK Tg(Htr3a-cre)NO152Gsat/Mmucd	UCD	RRID:MMRRC_036680-UCD
Software and Algorithms		
MATLAB	https://www.mathworks.com/products/matlab.html	RRID:SCR_001622
Labview	http://www.ni.com/labview/	RRID:SCR_014325
KiloSort	Jun et al., 2017 ; https://github.com/cortex-lab/KiloSort	N/A
Phy	Jun et al., 2017; https://github.com/kwikteam/phy	N/A